Optical Materials 52 (2016) 62–68

Contents lists available at ScienceDirect

Optical Materials

journal homepage: www.elsevier.com/locate/optmat

Tb^{3+}/Yb^{3+} codoped silica–hafnia glass and glass–ceramic waveguides to improve the efficiency of photovoltaic solar cells

A. Bouajaj [a], S. Belmokhtar [a], M.R. Britel [a], C. Armellini [b], B. Boulard [c], F. Belluomo [d], A. Di Stefano [d], S. Polizzi [e], A. Lukowiak [f], M. Ferrari [b], F. Enrichi [b,g,*]

[a] Laboratory of Innovative Technologies, LTI, ENSA–Tangier, University Abdelmalek Essaâdi, Tangier, Morocco
[b] CNR-IFN, Istituto di Fotonica e Nanotecnologie, CSMFO Lab and FBK Photonics Unit, Via alla Cascata 56/C, 38123 Povo (Trento), Italy
[c] Institut des Molécules et Matériaux du Mans, UMR 6283, Equipe Fluorures, Université du Maine, Av. Olivier Messiaen, 72085 Le Mans cedex 09, France
[d] Meridionale Impianti SpA, Via Senatore Simonetta 26/D, 20867 Caponago (MB), Italy
[e] Department of Molecular Sciences and Nanosystems, INSTN and Centro di Microscopia Elettronica "Giovanni Stevanato", Università Ca' Foscari Venezia, via Torino 155/b, 30172 Mestre (Venezia), Italy
[f] Institute of Low Temperature and Structure Research, PAS, ul. Okolna 2, 50-950 Wroclaw, Poland
[g] Veneto Nanotech, Laboratorio Nanofab, Via delle Industrie 5, 30125 Marghera (Venezia), Italy

ARTICLE INFO

Article history:
Received 9 October 2015
Received in revised form 2 December 2015
Accepted 9 December 2015

Keywords:
Glass–ceramic waveguides
Photoluminescence
Tb–Yb rare earths
Energy transfer
Quantum cutting
Solar cells

ABSTRACT

In this paper we present the investigation of the energy transfer efficiency between Tb^{3+} and Yb^{3+} ions in silica–hafnia waveguides. Cooperative energy transfer between these two ions allows to cut one 488 nm photon in two 980 nm photons and could have important applications in improving the performance of photovoltaic solar cells. Previous works revealed that for a given concentration of donors (Tb^{3+}), increasing the number of acceptors (Yb^{3+}) located near to the Tb^{3+} ion can increase the Tb–Yb transfer probability. However, when increasing the density of active ions, some detrimental effects due to cross-relaxation mechanisms become relevant. On the basis of this observation the sample doping was chosen keeping constant the molar ratio [Yb]/[Tb] = 4 and the total rare earths contents were [Tb + Yb]/[Si + Hf] = 5%, 7%, 9%. The choice of the matrix is another crucial point to obtain an efficient down conversion processes with rare earth ions. To this respect a $70SiO_2$–$30HfO_2$ waveguide composition was chosen. The comparison between the glass and the glass–ceramic structures demonstrated that the latter is more efficient since it combines the good optical properties of glasses with the optimal spectroscopic properties of crystals activated by luminescent species. A maximum transfer efficiency of 55% was found for the highest rare earth doping concentration.

1. Introduction

The absorption of radiation and its electrical conversion in photovoltaic solar cells is spectrally controlled by the bandgap of the semiconductor material. This corresponds, for instance, to 1127 nm for c-Si (Eg = 1.1 eV) or to 690 nm for amorphous silicon (a-Si, Eg = 1.8 eV) [1]. Radiation with energy lower than the bandgap is not absorbed because it is not able to generate electron–hole pairs and it is lost. Radiation with energy much higher than the gap is also not efficient because most of the energy is lost in internal thermalization processes [2]. Both of these losses are thus related to the spectral mismatch of the energy distribution of photons in the solar spectrum and the band gap of the semiconductor material and are the main sources of losses in PV solar cells. These phenomena lead to a loss in power of 24% by the non-absorption of low energy photons and 32% by thermalization [3]. Moreover thermalization also contributes to the heating of the photovoltaic cell which further reduces its performance [4].

After the "first generation" silicon wafer-based solar cells and the "second generation" of thin-film technology focused on lower material consumption, the evolution for "third generation" solar cells is based on the high efficiency conversion per unit area, with the possibility to double or even triple the energy conversion values from the present 15–20% to approach the thermodynamic limit upon solar conversion of 93% [5]. One of the keys to obtain high efficiency solar energy conversion is related to improving the match between the solar spectrum and the band gap of the semiconductor. This can be done either by adjusting the band gap of the device to the solar spectrum or by modifying the spectrum of the light that reaches the solar cell. The first approach is the case

* Corresponding author at: Veneto Nanotech, Laboratorio Nanofab, Via delle Industrie 5, 30125 Marghera (Venezia), Italy.
E-mail address: f.enrichi@gmail.com (F. Enrichi).

http://dx.doi.org/10.1016/j.optmat.2015.12.013
0925-3467/

of multi-junction cells which are a combination of several semiconductors. Each semiconductor has a different bandgap in order to collect a portion of the solar spectrum. The second approach, the wavelength conversion solution [6], uses luminescent materials for downconversion and upconversion processes (Fig. 1) in order to transfer as much of the solar photon energies close to the energy gap of the semiconductor, where absorption and efficiency of the device are maximum. Indeed, by concentrating the 300–1500 nm solar emission spectrum into a single narrow band spectrum corresponding to the bandgap the theoretical efficiency would be close to 80% [7].

This work is focused on this second approach, in particular on the development of downconverting materials [8,9]. The interest of these materials is that they can be easily integrated in the PV cells without changing their architecture, as a coating layer or by modifying some constituents of the cell itself like the encapsulating polymer or the cover glass. For this purpose different solutions have been proposed: metal sub-nanometric aggregates [10], quantum dots [11,12], plasmonic structures [13–15] or rare earth ions [12,16]. Rare earths are good candidates due to their wide variety of electronic levels [17]. The energy conversion by rare earths can be divided into three physical phenomena: quantum-cutting, down-shifting and up-conversion.

In this paper we focus on a quantum cutting mechanism which can produce two 980 nm photons from one 488 nm photon [18,19]. This process is based on a cooperative energy transfer mechanism between one Tb^{3+} and two Yb^{3+} rare earth ions. Yb^{3+} has only one excited level ($^2F_{5/2}$). The relaxation $^2F_{5/2} \rightarrow {}^2F_{7/2}$ between the excited state and the fundamental level produces a near infra-red (NIR) photon at 980 nm wavelength, which is close to the edge of silicon band gap. On the other hand Tb^{3+} is used as sensitizer, with absorption in the blue at 488 nm through the $^7F_6 \rightarrow {}^5D_4$ energy levels and cooperative transfer to Yb^{3+} ions (Fig. 2).

Sol gel-derived silica–hafnia is a reliable and flexible system suitable for rare earth doping and fabrication of glass–ceramic planar waveguides. In silica–hafnia glass–ceramic the rare earth ions are embedded in hafnia nanocrystals which have a cutoff frequency of about 700 cm^{-1}. Therefore, the presence of hafnia nanocrystals provides a strong reduction of the non-radiative transition processes and an increase of the measured emission lifetime. For these reasons the silica hafnia glass–ceramic is a suitable matrix to produce rare-earth activated films for downconversion. The wavelength downconversion layer is placed in front of the photovoltaic cell in order to transform the radiation energy spectrum before the semiconductor solar cell.

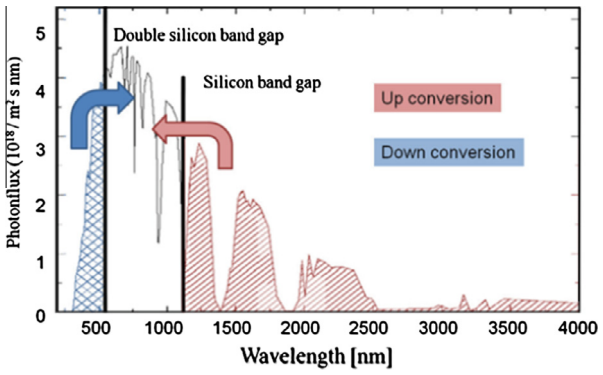

Fig. 1. Solar spectrum with the indication of the band gap and twice the band gap of silicon. The down-conversion and up-conversion processes convert photons respectively from a high and from a low energy range to the absorption band of silicon.

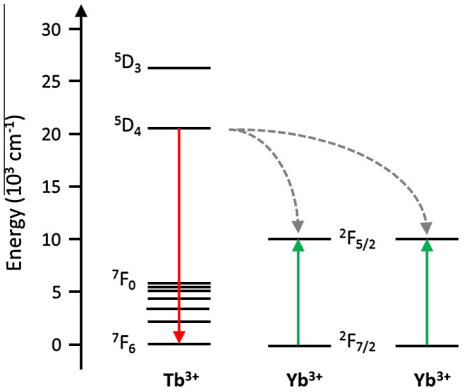

Fig. 2. The Tb^{3+}:$^5D_4$ energy level corresponds to about twice the energy of the Yb^{3+}:$^2F_{5/2}$ energy level. The cooperative energy transfer between a Tb^{3+} ion and two Yb^{3+}ions can generate two NIR photons, emitted by Yb^{3+} ions, after the absorption of a single photon by a Tb^{3+} ion.

Previous studies on $70SiO_2$–$30HfO_2$ downconverting waveguides [18,19] showed a transfer efficiency as high as 38% for glass–ceramic films activated by the maximum rare earth amount: 1% of terbium and 4% of ytterbium ([Yb + Tb] = 5%). These studies reported also that for a given concentration of donors (Tb^{3+}), increasing the number of acceptors (Yb^{3+}) located close to the Tb^{3+} ion can have detrimental effects due to concentration quenching. Therefore the optimal concentration rate resulted in [Yb]/[Tb] = 4.

In the current paper we compare two series of $70SiO_2$–$30HfO_2$ samples activated by different molar concentrations of rare earths [Tb + Yb]/[Si + Hf] = 5%, 7%, 9%, prepared by sol–gel route using the dip-coating technique. The two series of samples were in form of glass (G) or glass–ceramic (GC), depending on the final annealing treatment at 900 °C or 1000 °C respectively.

2. Experimental

Two series of $70SiO_2$–$30HfO_2$ samples activated by different molar concentrations of terbium and ytterbium ions were prepared by sol–gel route using the dip-coating technique, keeping constant the rate [Yb]/[Tb] = 4, following the experimental procedure described in [18,19]. Silica–hafnia films were deposited on cleaned pure SiO_2 substrates and the final films, obtained after 20 dips, were stabilized by a treatment of 5 min in air at 900 °C. As a result of the procedure, transparent and crack-free films were obtained (G samples). To obtain GC samples, an additional heat treatment was performed in air at a temperature of 1000 °C for 30 min in order to nucleate hafnia nanocrystals inside the film. $70SiO_2$–$30HfO_2$ GC planar waveguides doped with rare earth ions were thus produced. Table 1 gives the compositional and optical parameters of the obtained silica–hafnia G and GC planar waveguides.

The thickness of the waveguides and the refractive index at 632.8 and 543.5 nm were obtained by a m-lines apparatus (Metricon, model 2010) based on the prism coupling technique, using a Gadolinium Gallium Garnet (GGG) prism, with the setup reported in [20].

X-ray Diffraction (XRD) spectra were collected in continuous scan mode in the 2θ range 10–100°, with a scanning step of 0.1° and counting time of 60 s.

Transmission Electron Microscopy (TEM) images were taken at 300 kV with a JEOL 3010 instrument with an ultrahigh resolution (UHR) pole-piece (0.17 nm point resolution), equipped with a Gatan slow-scan CCD camera (model 794) and an Oxford Instrument EDS microanalysis detector (model 6636). X-ray Diffraction (XRD) measurements were carried out at room temperature by

Table 1
Rare earth concentration, refractive index and layer thickness of the prepared silica–hafnia G and GC waveguides.

Sample label	[Tb] (mol%)	[Yb] (mol%)	n@543.55 nm [±0.001]		n@632.8 nm [±0.001]		Layer thickness [±0.2 μm] (μm)
			TE_0	TM_0	TE_0	TM_0	
BR3G	1	0	1.589	1.576	1.575	1.561	0.7
BR3GC	1	0	1.599	1.583	1.585	1.568	0.7
B3G	1	4	1.590	1.580	1.578	1.565	0.7
B3GC	1	4	1.610	1.598	1.596	1.582	0.7
BR4G	1.4	0	1.578	1.569	1.566	1.558	0.8
BR4GC	1.4	0	1.591	1.579	1.579	1.565	0.7
B4G	1.4	5.6	1.592	1.581	1.579	1.566	0.7
B4GC	1.4	5.6	1.619	1.607	1.606	1.592	0.7
B5RG	1.8	0	1.602	1.590	1.590	1.576	0.7
B5RGC	1.8	0	1.611	1.592	1.597	1.576	0.7
B5G	1.8	7.2	1.589	1.577	1.577	1.565	0.8
B5GC	1.8	7.2	1.610	1.583	1.598	1.583	0.8

an X'Pert PRO diffractometer (Panalytical). A Cu anode (with Kα 1, 2 lines) was used as radiation source. Owing to the small thickness of the investigated waveguides, the grazing incidence X-ray diffraction (GIXRD) geometry was employed.

The transmittance spectra were recorded with an UV near-infrared spectrophotometer. The photo-luminescence characterization was performed by a Horiba JobinYvon Fluorolog-3 spectrofluorimeter, able to perform PL, PLE and time resolved PL measurements both in solid and liquid samples in the whole range of UV–VIS–NIR wavelengths (from 250 nm to 1700 nm). The light of a 450 W Xenon lamp excites the sample after passing a double-grating Czerny–Turner monochromator to select the desired wavelength. As an alternative, external lasers or LED sources can be used. The optical emission of the sample is analyzed by a single grating monochromator coupled to a suitable detector: a Hamamatsu PMT R928 for measurements between 185 nm and 900 nm or a PMTR5509-73 for measurements up to 1700 nm.

For the lifetime analysis the spectrofluorimeter was operated in Multi Channel Scaling (MCS) mode. The excitation source was a pulsed Nd:YAG laser at 1064 nm included in a complete system that incorporates non-linear crystals for the generation of photons at different energies. The system is the NT 342/3/UVE/AW of Ekspla, with selectable emission from 210 nm to 2300 nm and pulse duration of about 6 ns with a repetition frequency of 10 Hz. In our application the laser was set at 350 nm to investigate the decay dynamic of the $^5D_4 \rightarrow {}^7F_5$ transition of Tb^{3+} ions, with emission at 543.5 nm.

3. Results and discussion

Table 1 reports the optical parameters for the prepared samples. The waveguides have a thickness between 0.65 and 0.84 μm. The refractive indices measured in TE and TM polarization modes are equal within the experimental uncertainty, so the birefringence can be considered negligible.

The morphological and structural properties of the waveguides have been obtained by XRD and TEM measurements. The XRD analysis of various samples is reported in Fig. 3. The patterns refer to waveguides doped with 1% Tb^{3+} treated at 900 °C (G) and 1000 °C (GC) and to the GC samples doped with a total rare earth content of [Tb + Yb]/[Si + Hf] = 7%, 9%. All XRD spectra contain contributions from amorphous structures. In particular, the hump centered at $2\theta \approx 21°$ is a typical feature of a-SiO_2, originating from the silica substrate and from the SiO_2 component of the waveguides (70 mol%). According to XRD, the waveguides treated at 900 °C are fully amorphous. As clearly shown in Fig. 3(a), crystallization in the $70SiO_2$–$30HfO_2$ waveguide starts after heat treatment at 1000 °C for 30 min as documented by the presence

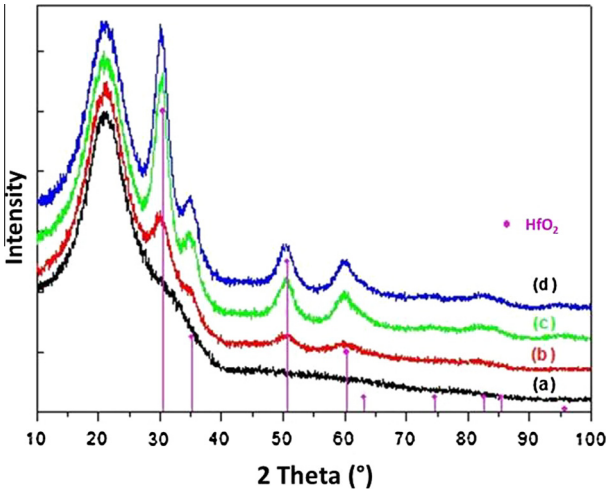

Fig. 3. XRD spectra of $70SiO_2$–$30HfO_2$ G and GC waveguides doped with different concentrations of Tb^{3+} and Yb^{3+}: (a) BR3G, (b) BR3GC, (c) B4GC, and (d) B5GC.

of Bragg reflection peaks. The effect of the crystallization increases by increasing the concentration of rare earths. Similar results were found by Gonçalves et al. in Er^{3+} doped $70SiO_2$–$30HfO_2$ planar waveguides [21]. From the comparison between XRD data and the ICSD database, we attribute the crystalline phase to the metastable tetragonal hafnium oxide (t-HfO_2). The diffraction peaks calculated from the matched ICSD card (No 85322) are shown (vertical lines), which belongs to the isostructural metastable t-HfO_2 phase. The evaluation of the crystal size by fitting of the peaks was in the range of 3–4 nm.

Fig. 4 shows the TEM images of the most doped G and GC samples, B5G and B5GC, with a total rare earth content of [Tb + Yb]/[Si + Hf] = 9%. The only difference in the two samples is the final annealing temperature at 900 °C or 1000 °C. It is worth observing that the sample treated at lower temperature is amorphous, while the higher temperature treatment induces the precipitation of small crystallites which size is of the order of 3–4 nm. This is fully in agreement with the XRD results previously discussed.

The optical transmission spectra of the investigated $70SiO_2$–$30HfO_2$ thin film doped with 1.4 mol% Tb^{3+} treated at 900 °C (BR4G) and treated at 1000 °C (BR4GC), not reported, reveal interference fringes due to the difference in refractive index between the v-SiO_2 slabs (n = 1.46 at 632.8 nm) as substrates and the G or GC layer ($n \sim 1.57$–1.60 at 632.8 nm). The transmittance of the GC is of the order of 90% in the visible and infrared regions; this high value is possible because of the small size of the precipitated crystals which is lower than visible light wavelength [22].

Photoluminescence emission of the samples was collected both in the visible and in the NIR spectral range. Fig. 5 shows, as an example, the photoluminescence excitation and emission of the Tb^{3+} doped GC sample BR5GC, with [Tb] = 1.8% in the visible range. The excitation spectrum (PLE) was obtained by monitoring the $^5D_4 \rightarrow {}^7F_5$ transition at λ_{em} = 543.5 nm. It consists of two parts: wavelengths lower than 330 nm and wavelengths higher than 330 nm. Below 330 nm it is in agreement with other works which reports two overlapping bands centered at maximum wavelengths of around 270 nm and 305 nm [23]. The origin of these bands is associated with the charge transfer (CT) from the orbitals 2p of O^{2-} to the 4f of Tb^{3+}, or with the 4f–5d intra-band transitions of Tb^{3+}. Beyond 330 nm the bands are due to 4f intra-band transitions of Tb^{3+} ions. The PL emission reports the characteristic $^5D_4 \rightarrow {}^7F_J$ transitions (J = 3, 4, 5, 6) of Tb^{3+}, with a maximum peak in the green at about 543.5 nm corresponding to the $^5D_4 \rightarrow {}^7F_5$ transition. The

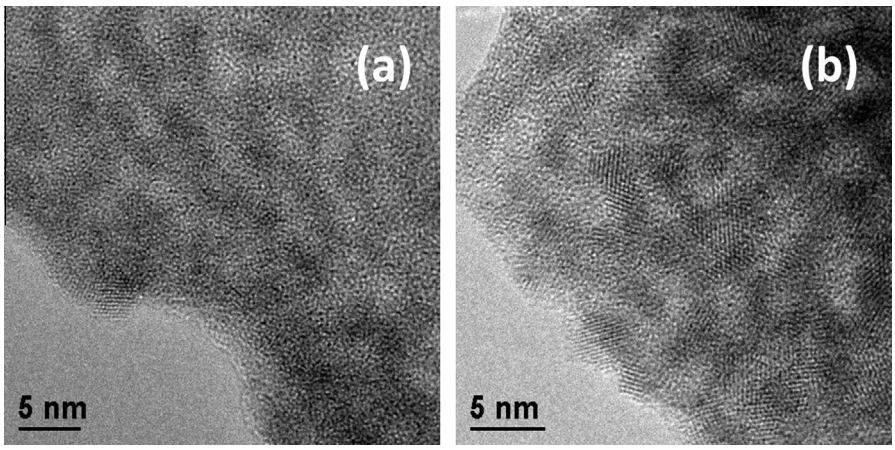

Fig. 4. TEM images of $70SiO_2$–$30HfO_2$ G and GC waveguides: (a) B5G, and (b) B5GC.

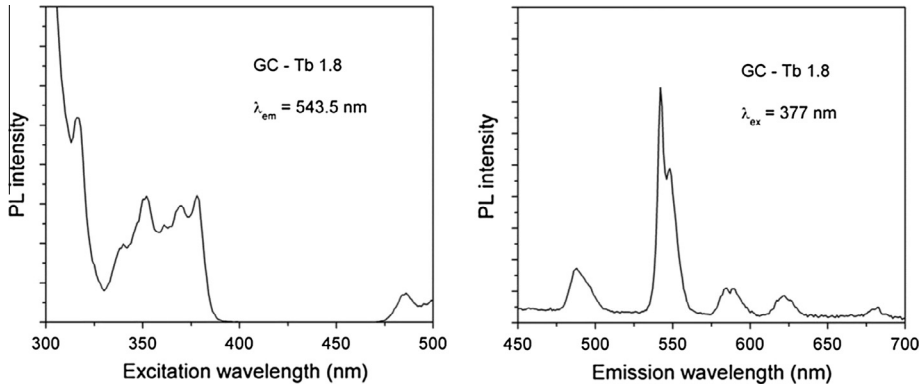

Fig. 5. PL excitation (left) and emission (right) of the representative BR5GC sample in the visible range.

comparison between the visible intensities of all the G and GC samples with or without Yb^{3+} ions is reported in Fig. 6. As expected in relation to the energy-transfer process, the introduction of Yb^{3+} acceptor ions strongly reduces the emission intensity from Tb^{3+} ions. Moreover, this effect is more significant for the GC samples with respect to the G samples. The analysis in the NIR is presented in Fig. 7 for the representative codoped GC sample B5GC, reporting the typical emission band peaked at 977 nm, with a shoulder at 1027 nm, attributed to the $^2F_{5/2} \rightarrow {}^2F_{7/2}$ transition of Yb^{3+} ions.

The conversion efficiency of the system is directly related to the energy transfer efficiency between $Tb^{3+}$and Yb^{3+}ions, which can be obtained by comparing the luminescence decay of terbium with and without ytterbium co-doping ions. Therefore the decay curves of the Tb^{3+} $^5D_4 \rightarrow {}^7F_5$ transition at 543.5 nm are plotted for the different samples in Fig. 8. Nearly single exponential luminescence decay is observed for the samples without Yb^{3+}, while faster luminescence decay with non-exponential behavior is typically observed for codoped samples. The lifetime reduction is attributed to the energy transfer from the Tb^{3+}:$^5D_4$ to the Yb^{3+}:$^2F_{5/2}$, where the non-exponential behavior of the decay is in perfect agreement with the Inokuti–Hirayama model [24]. From a graphical comparison, it is worth observing that the GC samples exhibit a much higher reduction in the lifetime with respect to the G samples. This is in agreement with the previous observation that we have done

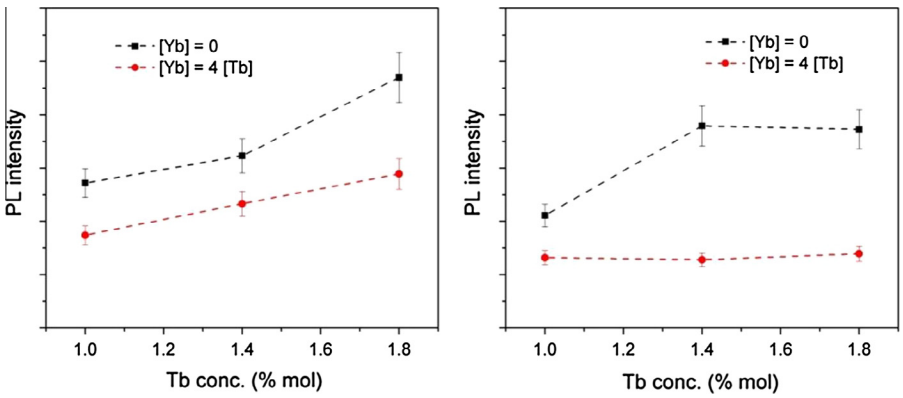

Fig. 6. PL intensities of all the G (left) and GC (right) samples in the visible range at $\lambda = 543.5$ nm.

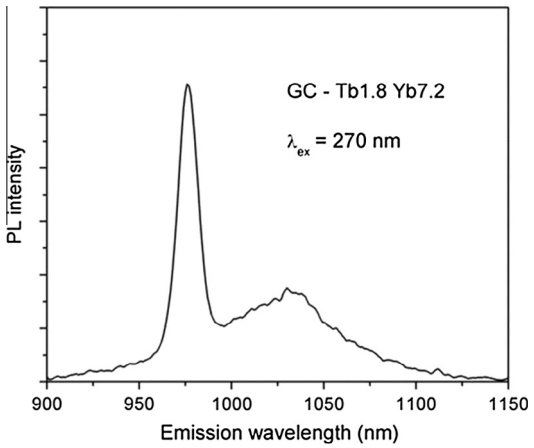

Fig. 7. PL emission of a representative GC sample in the NIR range.

regarding the 543.5 nm PL intensity reduction reported in Fig. 6. Moreover, within each family, a very significant change occurs for the highest rare earths concentration of 9% with respect to the lower concentrations of 5% and 7%. This behavior can be quantified by single exponential fitting of the curves or, where necessary, double exponential fitting followed by evaluation of average lifetime [25]. The average lifetime of the Tb^{3+} $^5D_4 \rightarrow {}^7F_5$ transition at 543.5 nm emission ions is reported in Table 2 for G samples and in Table 3 for GC samples. It is worth observing that the measured lifetime is almost independent from Tb^{3+} concentration in the single doped samples without Yb^{3+}. Moreover it is longer for the GC samples (around 2.7 ms) with respect to G samples (about 2.1 ms) in agreement with the rare earth confinement in the HfO_2 crystal which has less non-radiative transition processes. After incorporation of Yb^{3+} the lifetime is strongly reduced as previously observed and the effect is more evident in the GC samples.

The energy transfer efficiency η_{Tb-Yb} can be calculated experimentally by dividing the integrated intensity of the decay curves of the Tb^{3+}–Yb^{3+}co-doped samples by the integrated intensity of the Tb^{3+} single doped curve [15,16]:

$$\eta_{Tb-Yb} = 1 - \frac{\int I_{Tb-Yb}\, dt}{\int I_{Tb}\, dt}$$

In some papers, effective quantum efficiency is employed, defined by the ratio between the number of emitted photons and the number of photons absorbed by the material. In our case, a perfect down-conversion system would have an effective quantum

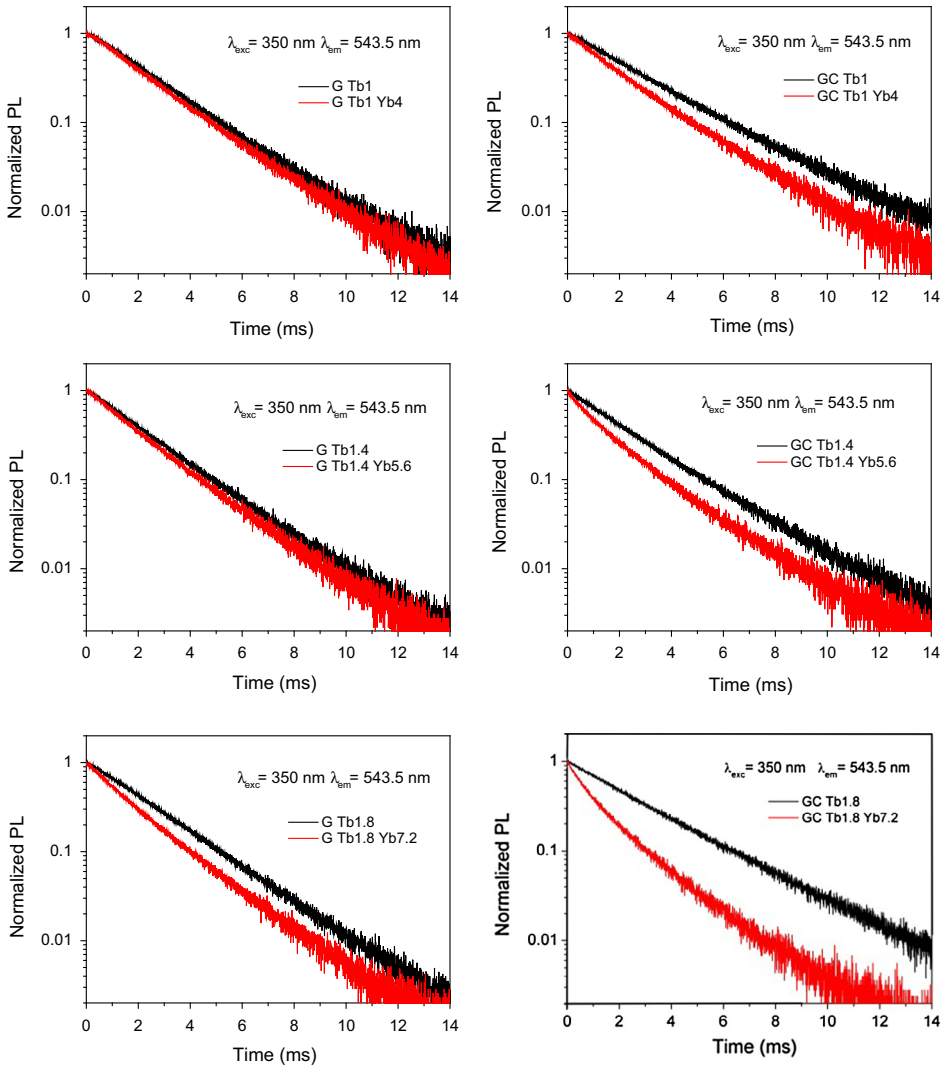

Fig. 8. Time resolved photoluminescence of the different G (left column) and GC (right column) samples at 543.5 nm emission under 350 nm excitation.

Table 2
Average lifetime τ (ms) of the Tb^{3+} $^5D_4 \rightarrow {}^7F_5$ transition @ 543.5 nm for G samples.

[Tb] in mol%	[Yb] = 0	[Yb] = 4 [Tb]
1	2.21	2.07
1.4	2.11	1.93
1.8	2.21	1.82

Table 3
Average lifetime τ (ms) of the Tb^{3+} $^5D_4 \rightarrow {}^7F_5$ transition @ 543.5 nm for GC samples.

[Tb] in mol%	[Yb] = 0	[Yb] = 4 [Tb]
1	2.69	2.17
1.4	2.35	1.83
1.8	2.72	1.52

Table 4
Transfer efficiency and effective quantum efficiency as function of [Tb + Yb] molar concentration for G samples with constant molar ratio Yb/Tb = 4.

Composition ([Tb + Yb] in mol%)	5	7	9
Transfer efficiency (%)	8.4	10.3	26.4
Effective quantum efficiency (%)	108.4	110.3	126.4

Table 5
Transfer efficiency and effective quantum efficiency as function of [Tb + Yb] molar concentration for GC samples with constant molar ratio Yb/Tb = 4.

Composition ([Tb + Yb] in mol%)	5	7	9
Transfer efficiency (%)	24.6	32.3	54.6
Effective quantum efficiency (%)	124.6	132.3	154.6

efficiency value of 200%, corresponding to the emission of two photons for one absorbed. The relation between the transfer efficiency and the effective quantum efficiency is linear and is defined as:

$$\eta_{EQE} = \eta_{Tb-r}(1 - \eta_{Tb-Yb}) + 2\eta_{Tb-Yb}$$

where the quantum efficiency for Tb^{3+} ions, η_{Tb-r}, is set equal to 1. The values of energy transfer efficiency and effective quantum efficiency calculated from the decay curves for the G samples are reported in Table 4, while the results for the GC samples are reported in Table 5. The values reported in the tables confirm the previous qualitative observations. In particular the transfer efficiency for GC samples is 2–3 times higher than the one of G samples. Moreover the transfer efficiency increases with the total rare earth content, confirming the trend reported in previous papers, with a highest value for the [Tb + Yb] = 9% in about 55%.

4. Conclusions

In summary, efficient quantum cutting in Tb^{3+}:Yb^{3+} co-doped $70SiO_2$–$30HfO_2$ glass and glass–ceramic waveguides deposited by a sol–gel route is reported in this paper. A fixed concentration rate [Yb]/[Tb] = 4 and increasing rare earths total amounts [Tb + Yb] = 5%, 7%, 9% have been studied. Structural investigation by XRD and TEM shows that the precipitation of small hafnia nanocrystals (size about 3–4 nm) in an amorphous silica matrix occurs after a thermal treatment at 1000 °C for 30 min. in air, while the same process at 900 °C is not enough for inducing phase separation and crystallization.

The waveguiding properties of the films are confirmed and a clear NIR photoluminescence emission around 980 nm is detected, due to the $^2F_{5/2} \rightarrow {}^2F_{7/2}$ transition of Yb^{3+} ions. The energy transfer efficiency, estimated from the PL decay curves of the $^5D_4 \rightarrow {}^7F_5$ transition at 543.5 nm of Tb^{3+} ions, increases when increasing the total [Tb + Yb] concentration. The best performance is almost 55% and it is obtained for the most doped glass–ceramic sample, while it is only 26% in the glass sample with the same rare earth concentration. Indeed, as a general observation, the glass–ceramic structure always increases the effective quantum efficiency compared to the parent glass for each concentration.

The waveguide configuration, because of the possibility to obtain high radiation confinement, opens new possibilities for integration of down-converters and light concentrators in PV solar cells.

Acknowledgements

The research activity was performed in the framework of the CNR-CNRST joint project (2014–2015), CNR-PAS joint project (2014–2016), and COST Action MP1401 (2014–2018).

References

[1] W.G.J.H.M. van Sark, L. Korte, F. Roca, Physics and Technology of Amorphous-Crystalline Heterostructure Silicon Solar Cells, Springer-Verlag, Berlin Heidelberg, 2012.
[2] B.S. Richards, Enhancing the performance of silicon solar cells via the application of passive luminescence conversion layers, Sol. Energy Mater. Sol. Cells 90 (2006) 2329–2337.
[3] M. Florescu, H. Lee, I. Puscasu, M. Pralle, L. Florescu, D.Z. Ting, J.P. Dowling, Improving solar cell efficiency using photonic band-gap materials, Sol. Energy Mater. Sol. Cells 91 (2007) 1599–1610.
[4] D. Meneses-Rodrıguez, P.P. Horley, J. González-Hernández, Y.V. Vorobiev, P.N. Gorley, Photovoltaic solar cells performance at elevated temperatures, Sol. Energy 78 (2005) 243–250.
[5] M.A. Green, Third Generation Photovoltaics: Advanced Solar Energy Conversion, Springer-Verlag, Berlin Heidelberg, 2003.
[6] C. Strumpel, M. McCann, G. Beaucarne, V. Arkhipov, A. Slaoui, V. Svrcek, C. del Cañizo, I. Tobias, Modifying the solar spectrum to enhance silicon solar cell efficiency – an overview of available materials, Sol. Energy Mater. Sol. Cells 91 (2007) 238–249.
[7] W.G.J.H. Van Sark, A. Meijerink, R.E.I. Schropp, Nanoparticles for solar spectrum conversion, Proc. SPIE 7772 (2010) 777206.
[8] T. Trupke, M.A. Green, P. Wurfel, Improving solar cell efficiencies by down-conversion of high-energy photons, J. Appl. Phys. 92 (2002) 1668–1674.
[9] B.S. Richards, Luminescent layers for enhanced silicon solar cell performance: down-conversion, Sol. Energy Mater. Sol. Cells 90 (2006) 1189–1207.
[10] E. Cattaruzza, V.M. Caselli, M. Mardegan, F. Gonella, G. Bottaro, A. Quaranta, G. Valotto, F. Enrichi, $Ag^+ \leftrightarrow Na^+$ ion exchanged silicate glasses for solar cells covering: down-shifting properties, Ceram. Int. 41 (2015) 7221–7226.
[11] Van Sark, Enhancement of solar cell performance by employing planar spectral converters, Appl. Phys. Lett. 87 (2005) 151117.
[12] S. Das, K.C. Mandal, Optical downconversion in rare earth (Tb^{3+} and Yb^{3+}) doped CdS nanocrystals, Mater. Lett. 66 (2012) 46–49.
[13] H.A. Atwater, A. Polman, Plasmonics for improved photovoltaic devices, Nat. Mater. 9 (2010) 205–213.
[14] S. Pillai, M.A. Green, Plasmonics for photovoltaic applications, Sol. Energy Mater. Sol. Cells 94 (2010) 1481–1486.
[15] V.E. Ferry, J.N. Munday, H.A. Atwater, Design considerations for plasmonic photovoltaics, Adv. Mater. 22 (2010) 4794–4808.
[16] A. Meijerink, R. Wegh, P. Vergeer, T. Vlugt, Photon management with lanthanides, Opt. Mater. 28 (2006) 575–581.
[17] G. Liu, B. Jacquier, Spectroscopic Properties of Rare Earths in Optical Materials, Springer-Verlag, Berlin Heidelberg, 2005.
[18] G. Alombert-Goget, C. Armellini, A. Chiappini, A. Chiasera, M. Ferrari, S. Berneschi, M. Brenci, S. Pelli, G.C. Righini, M. Bregoli, A. Maglione, G. Pucker, G. Speranza, Frequency converter layers based on terbium and ytterbium activated HfO_2 glass–ceramics, Proc. SPIE 7598 (2010). 75980P–1/9.
[19] G. Alombert-Goget, C. Armellini, S. Berneschi, A. Chiappini, A. Chiasera, M. Ferrari, S. Guddala, E. Moser, S. Pelli, D.N. Rao, G.C. Righini, Tb^{3+}/Yb^{3+} co-activated Silica–Hafnia glass ceramic waveguides, Opt. Mater. 33 (2010) 227–230.
[20] S. Ronchin, A. Chiasera, M. Montagna, R. Rolli, C. Tosello, S. Pelli, G.C. Righini, R. R. Goncalves, S.J.L. Ribeiro, C.S. De Bernardi, F. Pozzi, C. Duverger, R. Belli, M. Ferrari, Erbium-activated silica–titania planar waveguides prepared by rf-sputtering, SPIE 4282 (2001) 31.
[21] R.R. Gonçalves, G. Carturan, L. Zampedri, M. Ferrari, M. Montagna, A. Chiasera, G.C. Righini, S. Pelli, S.J.L. Ribeiro, Y. Messaddeq, Sol–gel Er-doped SiO_2–HfO_2 planar waveguides: a viable system for 1.5 μm application, Appl. Phys. Lett. 81 (1) (2002) 28–30.
[22] Y. Jestin, C. Armellini, A. Chiappini, A. Chiasera, M. Ferrari, C. Goyes, M. Montagna, E. Moser, G. Nunzi Conti, S. Pelli, R. Retoux, G.C. Righini, G. Speranza, Erbium activated HfO_2-based glass–ceramics waveguides for photonics, J. Non-Cryst. Solids 353 (2007) 494–497.

[23] M. Back, A. Massari, M. Boffelli, F. Gonella, P. Riello, D. Cristofori, R. Riccò, F. Enrichi, Optical investigation of Tb^{3+}-doped Y_2O_3 nanocrystals prepared by Pechini-type sol–gel process, J. Nanopart. Res. 14 (2012) 792–801.

[24] L. Fu, H. Xia, Y. Dong, S. Li, H. Jiang, B. Chen, Cooperative down-conversion luminescence in Tb^{3+}/Yb^{3+} co-doped $LiYF_4$ single crystals, IEEE Photonics J. 6 (1) (2014) 1–9.

[25] R. Marin, G. Sponchia, E. Zucchetta, P. Riello, F. Enrichi, G. De Portu, A. Benedetti, Photoluminescence properties of YAG:Ce^{3+}, Pr^{3+} phosphors synthesized via the Pechini method for white LEDs, J. Am. Ceram. Soc. 96 (2013) 2628–2635.